Excitation spectra of aromatic molecules within a real-space GW-BSE formalism: Role of self-consistency and vertex corrections

Linda Hung, Felipe H. da Jornada, Jaime Souto-Casares, James R. Chelikowsky, Steven G. Louie, and Serdar Öğüt

Phys. Rev. B **94**, 085125 — Published 15 August 2016

DOI: 10.1103/PhysRevB.94.085125

Excitation spectra of aromatic molecules within a real-space GW-BSE formalism: the role of self-consistency and vertex corrections

Linda Hung,[1,2,*] Felipe H. da Jornada,[3,4] Jaime Souto-Casares,[5]
James R. Chelikowsky,[5,6,7] Steven G. Louie,[3,4] and Serdar Öğüt[1,†]

[1] *Department of Physics, University of Illinois at Chicago, Chicago, Illinois 60607, USA*
[2] *NIST Center for Neutron Research, National Institute of Standard and Technology, Gaithersburg, MD, 20899, USA*
[3] *Department of Physics, University of California, Berkeley, California 94720, USA*
[4] *Materials Sciences Division, Lawrence Berkeley National Laboratory, Berkeley, California 94720, USA*
[5] *Center for Computational Materials, Institute for Computational Engineering and Sciences, The University of Texas at Austin, Austin, Texas 78712, USA*
[6] *Department of Chemical Engineering, The University of Texas at Austin, Austin, Texas 78712, USA*
[7] *Department of Physics, The University of Texas at Austin, Austin, Texas 78712, USA*

We present first-principle calculations on the vertical ionization potentials (IPs), electron affinities (EAs), and singlet excitation energies on an aromatic-molecule test set (benzene, thiophene, 1,2,5-thiadiazole, naphthalene, benzothiazole, and tetrathiafulvalene) within the *GW* and Bethe-Salpeter equation (BSE) formalisms. Our computational framework, which employs a real-space basis for ground-state and a transition-space basis for excited-state calculations, is well-suited for high-accuracy calculations on molecules, as we show by comparing against G_0W_0 calculations within a plane-wave-basis formalism. We then generalize our framework to test variants of the *GW* approximation that include a local-density approximation (LDA)-derived vertex function (Γ_{LDA}) and quasiparticle-self-consistent (QS) iterations. We find that Γ_{LDA} and quasiparticle self-consistency shift IPs and EAs by roughly the same magnitude, but with opposite sign for IPs and same sign for EAs. G_0W_0 and QS$GW\Gamma_{\mathrm{LDA}}$ are more accurate for IPs, while $G_0W_0\Gamma_{\mathrm{LDA}}$ and QSGW are best for EAs. For optical excitations, we find that perturbative *GW*-BSE underestimates the singlet excitation energy, while self-consistent *GW*-BSE results in good agreement with previous best-estimate values for both valence and Rydberg excitations. Finally, our work suggests that a hybrid approach, where G_0W_0 energies are used for occupied orbitals and $G_0W_0\Gamma_{\mathrm{LDA}}$ for unoccupied orbitals, also yields optical excitation energies in good agreement with experiment but at a smaller computational cost.

I. INTRODUCTION

Green's function methods, such as the *GW* approximation and the Bethe-Salpeter equation (BSE), are most commonly used in the calculation of one- and two-particle excitations in condensed matter, but have been increasingly applied in the study of molecules. The *GW* approximation allows one to solve for the interacting one-particle Green's function, whose poles are associated with vertical ionization potentials (IPs) and electron affinities (EAs). The BSE, on the other hand, allows one to construct an interacting two-particle correlation function from previously-determined one-particle Green's functions; the poles of the two-particle Green's function are associated with neutral excited states such as those observed in optical and electron energy loss experiments. The computational efficiency of these methods enables the simulation of excited-state properties in large molecules and clusters, and the benchmarks across a variety of *sp*-bonded and transition-metal oxide molecules are now available.[1–24]

In theory, intrinsic IPs and EAs can be determined exactly from the one-particle Green's function by fully solving Hedin's equations.[25] Similarly, it is possible to obtain exact neutral excitations by solving the BSE, starting from the exact one-particle Green's functions and including the exact electron-hole interaction kernel. Unfortunately, obtaining the self-consistent solution to Hedin's equation is computationally infeasible. As is discussed in Sec. II A, the *GW* approximation is commonly used instead, where the three-point vertex function Γ is changed to a computationally tractable Dirac delta function. A second approximation arises when *GW* equations are not solved self-consistently, but are instead computed as a perturbation to a mean-field solution, *e.g.*, Kohn-Sham density-functional theory (DFT) or Hartree-Fock. As a result, *GW* and *GW*-BSE benchmarks exhibit errors that have been primarily attributed to some combination of the vertex approximation and the non-self-consistency of its solutions.

In addition, the accuracy of first-principles results are affected by the numerical framework of the calculation. For molecules, this is highlighted by the difficulty in representing resonant and continuum unoccupied orbitals. Even a small isolated molecule has excitations involving diffuse and unbound orbitals with large spatial ranges. Therefore, any numerical approximation associated with the choice of basis set must be carefully weighed against the overall computational cost, whether a simulation applies a local atomic orbital basis set, periodic boundary conditions, or confined boundary conditions (where the wave function amplitudes are set to zero at and beyond the boundary).

In this work, we explore the numerical and theoretical contributions to the performance of the *GW* ap-

proximation and the BSE on an aromatic-molecule test set. The molecules, comprising benzene (C_6H_6), thiophene (C_4H_4S), 1,2,5-thiadiazole ($C_2H_2N_2S$), naphthalene ($C_{10}H_8$), benzothiazole (C_7H_5NS), and tetrathiafulvalene (TTF, $C_6H_4S_4$), have applications as building blocks in modern functional materials such as organic semiconductors and organic frameworks. The test set includes orbitals with σ, π, lone pair, and continuum character, whose differing physical characteristics provide a diverse set of challenges to our first-principles methods. We check the numerical convergence of occupied and low-lying unoccupied orbitals by comparing calculations on a real-space grid with confined boundary conditions, which use a transition-space basis for excited-state calculations,[26,27] to computations on a plane-wave basis in repeated supercells with periodic boundary conditions.[28,29] We then use the real-space framework to examine how the vertex function and self consistency affect the accuracy of *GW* predictions, benchmarking *GW* energies at four levels of theory: G_0W_0, $G_0W_0\Gamma_{\mathrm{LDA}}$, QS$GW$, and QS$GW\Gamma_{\mathrm{LDA}}$. Perturbative "one-shot" calculations are denoted by G_0W_0 and $G_0W_0\Gamma_{\mathrm{LDA}}$, and quasiparticle-self-consistent (QS)[30] *GW* calculations are denoted by QSGW and QS$GW\Gamma_{\mathrm{LDA}}$; Γ_{LDA} indicates the inclusion of a local density approximation (LDA)-derived vertex in the calculation.[31] The energies of singlet (optical) excitations are computed by solving the BSE based on results from each level of *GW* theory. Time-dependent DFT (TDDFT) calculations with the adiabatic LDA exchange-correlation functional, denoted by TDLDA, are presented as well. All calculations in this work start from the same mean-field electronic structure: DFT with the LDA exchange-correlation functional.

We begin this article with an overview of the *GW* approximation of the one-particle Green's functions, and the BSE solutions of two-particle correlation functions. We then describe the computational setup for our calculations and validate the numerical accuracy of our combined real- and transition-space implementation of the *GW* approximation by comparison to calculations with a fully plane-wave framework. Finally, we benchmark the accuracy of one-particle Green's functions obtained at various levels of *GW* theory, as well as the BSE predictions built upon these Green's functions, and discuss the effects of the vertex function and self-consistent *GW* on predictions of IPs, EAs, and neutral singlet excitation energies.

II. THEORY

A. One-particle Green's function

The one-electron excitation spectrum, associated with the removal or addition of an electron to a system, can be obtained from the one-particle Green's function G. When the chemical potential is set at the vacuum level, quasiparticle energies are given by ε_i, the positions of the poles of G. IPs are predicted by $-\varepsilon_i$ for quasiparticles corresponding to the energy needed to remove electrons (from occupied states), while EAs are predicted by $-\varepsilon_i$ for quasiparticles corresponding to the energy gained by the system when adding an electron (to unoccupied states). Note that we use somewhat unconventional terminology: IP indicates the binding energy for any electron in the neutral molecule (not just the most loosely-bound electron), and EA indicates the energy released when adding an electron to any unoccupied orbital (not just the lowest-lying unoccupied orbital), *i.e.*, IPs are the excitation energies of creating holes, and EAs are the excitation energies of creating quasielectrons.

For spatial coordinates $\mathbf{r}$, $\mathbf{r}'$, $\mathbf{r}''$, and energy ω, G satisfies the equation of motion

$$[\omega - H_0(\mathbf{r})]G(\mathbf{r},\mathbf{r}',\omega) - \int d^3\mathbf{r}''\Delta\Sigma(\mathbf{r},\mathbf{r}'',\omega)G(\mathbf{r}'',\mathbf{r}',\omega) = \delta(\mathbf{r},\mathbf{r}'), \tag{1}$$

where δ is the Dirac delta function and

$$H_0 = -\frac{1}{2}\nabla^2 + V_H(\mathbf{r}) + V_0(\mathbf{r}) \tag{2}$$

is a mean-field Hamiltonian composed of the kinetic energy operator, the Hartree (Coulomb) potential V_H, and a local external potential V_0. Contributions to the external potential can include the ionic potential and a mean-field exchange-correlation potential, and $\Delta\Sigma$ is the difference between the self energy Σ and the exchange-correlation contribution from H_0. For the specific case of a DFT-LDA mean-field Hamiltonian with corresponding exchange-correlation potential V_{xc},

$$\Delta\Sigma(\mathbf{r},\mathbf{r}',\omega) = \Sigma(\mathbf{r},\mathbf{r}',\omega) - V_{\mathrm{xc}}(\mathbf{r})\delta(\mathbf{r},\mathbf{r}'). \tag{3}$$

The mean-field Green's function G_0 that corresponds to the solution of Equation 1 when $\Delta\Sigma = 0$ is used in the Dyson equation for G,

$$G(12) = G_0(12) + \int d(34)G_0(13)\Delta\Sigma(34)G(42), \tag{4}$$

in which space-time variables are expressed in many-body notation: $1 \equiv (\mathbf{r}_1, t_1)$. To obtain the interacting one-electron Green's function, the Dyson equation above can be solved self-consistently with the following equations:

$$\chi(12) = -i\int d(34)G(13)\Gamma(34,2)G(41^+), \tag{5}$$

$$W(12) = V_H(12) + \int d(34)V_H(13)\chi(34)W(42), \tag{6}$$

$$\Sigma(12) = i\int d(34)G(13)W(41^+)\Gamma(32,4), \tag{7}$$

and

$$\Gamma(12,3) = \delta(12)\delta(13) + \int d(4567)\frac{\delta\Sigma(12)}{\delta G(45)}G(46)G(75)\Gamma(67,3), \quad (8)$$

where χ is the polarizability, W is the screened Coulomb interaction, Γ is the vertex function, and 1^+ denotes that $t \to t + \delta$ for some positive infinitesimal δ.

In the GW approximation,[25] the one-particle Green's function is still solved via Equations 4-7, but the vertex function is approximated as

$$\Gamma(12,3) = \delta(12)\delta(13). \quad (9)$$

This approximation removes the need to evaluate a four-point integral and is equivalent to expanding the Green's function to the first order in terms of the screened Coulomb interaction.

Apart from this conventional GW approximation, other approximate vertex functions have been derived to include certain higher-order terms[32–40] or to reflect the response of density functionals.[31,41–47] In the density functional approach, the polarizability (Eq. 5) is expressed within TDDFT. A consistent level of approximation is maintained by replacing Eq. 8 with

$$\Gamma(12,3) = \delta(12)\delta(13) - i\delta(12)f_{\text{xc}}(1)\int d(45)G(14)G(51^+)\Gamma(45,3), \quad (10)$$

where the expression above assumes that the exchange-correlation kernel $f_{\text{xc}} = \frac{\delta V_{\text{xc}}}{\delta\rho}$ is local. This is the form of the LDA-derived vertex (Γ_{LDA}) used in this work. While past results indicate that Γ_{LDA} is still a rough approximation for the true vertex, and the relative energy level spacings are unchanged by Γ_{LDA},[31,48] here we apply Γ_{LDA} to benchmark the absolute accuracy for quasiparticle energies.

In addition to the vertex approximation in GW, a second approximation is often applied by computing a perturbative result (G_0W_0) instead of a self-consistent one; only one cycle through the equations above is added onto the initial mean-field approximation. The choice of the starting mean-field picture therefore impacts the accuracy of the G_0W_0 prediction, as reflected in several benchmarks of molecular systems.[8,11,21] Compared to G_0W_0, self-consistent GW solutions have certain advantages, including starting-point independence, fulfillment of energy and momentum conservation laws, and consistent values for observables when using different partitioning functions.[49] Self-consistent GW therefore produces good results when studying ground-state properties.[50–53] The spectral properties of extended systems, however, appear to be poorly described by self consistent GW, with band energies worse than perturbative calculations and valence bandwidth too large.[50,53,54] These self-consistent results demonstrate the full impact of approximating the vertex function in extended systems; perturbative GW results for spectral properties apparently benefit from some counteracting effects between the vertex function and self-consistency.[35,36] On the other hand, self-consistent GW appears to be better suited to describing spectral properties for finite systems like atoms and molecules. In several examples with atom-centered basis sets, the accuracy of self-consistent GW is competitive with G_0W_0 predictions using Hartree-Fock and hybrid functional mean-field starting points.[2–5,10,13,15,17,22,24,52,55] However, recent results for fully self-consistent GW on a plane-wave basis set report slightly larger errors.[19] Overall, self-consistent GW pushes the IPs upward compared to G_0W_0 with a DFT starting point, and it shifts IPs slightly downward when using a Hartree-Fock starting point.

Interpreting these varying benchmarks for self-consistent GW is complicated due to additional approximations in the implementation of self-consistency. Many calculations use eigenvalue self-consistency or the "diagonal approximation", where quasiparticle wave functions remain fixed as the mean-field wave functions. For fully self-consistent and QSGW, however, the wave functions are optimized as well. In QSGW,[30] the GW self-energy is used to construct a better approximation for the mean-field effective potential $V_{\text{xc}}(\mathbf{r},\mathbf{r}')$ (generalizing Equations 2 and 3), which is in turn used to build a new set of mean-field Green's functions. Using the new Green's functions, the cycle (including updates to W) is repeated until self-consistency is reached between the mean-field and the new G_0W_0 Green's functions. The accuracy of QSGW and fully self-consistent GW appear to be comparable for molecules,[15] and in this work, we study self-consistency in the form of QSGW.

B. Two-particle correlation function

The two-particle correlation function L associated with the interacting two-particle Green's function is the solution to the BSE, and can be used to understand response functions associated to neutral excitations. In its spectral form, L is written in terms of normalized eigenvectors A^l and poles at energy Ω_l, which can be associated to optical excitation energies. As a result, the absorption cross section $\sigma(E)$ is expressed in terms of these quantities by summing over the eigenvectors index l and Cartesian directions $\beta = \{x, y, z\}$:

$$\sigma(E) = \frac{8\pi^2 e^2}{3c}\sum_{l\,\beta}\left[\Omega_l\left(\int d\mathbf{r}\rho_l(\mathbf{r})\beta\right)^2\delta(E-\Omega_l)\right], \quad (11)$$

with

$$\rho_l(\mathbf{r}) = \sum_{vc}\varphi_c(\mathbf{r})\varphi_v(\mathbf{r})A^l_{vc}, \quad (12)$$

where φ_c and φ_v are the wave functions associated to the quasiparticle that make up the exciton.

The BSE can be cast into a Dyson equation for L as

$$L(12,34) = L^0(12,34) + \int d(5678) L^0(12,56) K(56,78) L(78,34), \tag{13}$$

where

$$L^0(12,34) = G(13)G(24), \tag{14}$$

with G being the one-particle Green's function. The electron-hole interaction kernel can be expressed as

$$K(56,78) = V_H(57)\delta(56)\delta(78) + \frac{\partial \Sigma(56)}{\partial G(78)}. \tag{15}$$

For computational efficiency, the energy dependence of K is typically left out of standard GW-BSE calculations, and we do the same in this work. Physically, the screening should be evaluated at the frequency corresponding to that of the exciton binding energy, which is in general a small fraction of the excitation energy of the molecule. Therefore, the use of static screening is a good approximation. Dynamical effects also appear to be canceled by high-order vertex corrections left out of standard GW.[56,57]

Finally, from the equations above, we see that the quality of the two-particle correlation function obtained from the BSE is completely dependent on the quality of G as well as the approximations to the kernel. In the GW-BSE formalism,[41,58] G is determined via the GW approximation. We also note that TDDFT calculations can be viewed in a BSE framework. In Casida's equations for linear-response TDDFT,[59] G is constructed from Kohn-Sham DFT wave functions and energies (instead of GW quasiparticle wave functions and energies), and $\frac{\partial \Sigma(56)}{\partial G(78)} \equiv f_{\text{xc}}$. Further similarities between GW-BSE and TDDFT have been discussed in Ref. 60.

III. COMPUTATION

A. Real-space vs. plane-wave implementations

The first-principles results presented in this work are computed using a real-space discrete grid and transition-space formalism for ground-state and excited-state calculations, respectively, and are validated by comparison to G_0W_0 calculations using a plane-wave basis set formalism. For all calculations, Kohn-Sham DFT-LDA is the mean-field starting point, and molecular geometries are optimized in PARSEC.[26] In addition, all calculations use the same Trouiller-Martins norm-conserving pseudopotentials generated within APE.[61] Although the pseudopotential approximation neglects core polarization effects and core-valence interactions, we expect the associated errors to be small on our particular test set (< 100 meV error), since core electrons are tightly bound.[62] Additional information about pseudopotential and molecular geometries are available in our Supplemental Material.

Since real-space and plane-wave calculations are performed at the same level of theory, the comparison of

TABLE I. Comparison of real-space (second column) and plane-wave (third column) frameworks for the GW calculations performed in this work. Wave functions in the real-space basis are represented on a sphere of radius R with grid spacing h_{grid}, while wave functions in the plane-wave basis are described in a cuboid boxes of sizes L_i and with plane-wave cutoff energy E^{ψ}_{cut}. We denote by N the overall system size, by N_{tot} the index of the highest-energy Kohn-Sham state included in GW summations, by N_{freq} and E^{χ}_{cut} the number of frequencies and the cutoff for plane-wave coefficients that represent the dielectric matrix, respectively, and by ΔE the energy spacing between two evaluations of $\Sigma(E)$.

Mean-field calculation: E_{DFT}, ψ_{DFT}		
Software	PARSEC	Quantum ESPRESSO
Boundary conditions	Confined: $\psi(\mathbf{r}_b) = 0$	Periodic: in phase (k=0)
Wave-function basis	Real-space grid	Plane waves
GW calculation: Σ, G, W		
Software	RGWBS	BerkeleyGW
Spatial basis for χ	Orbitals	Plane waves
Dynamical descript. of χ	Lehmann/spectral representation	Explicit calc. at various freqs.
Σ integration	Sum over all poles	Contour deform. formalism
Quasiparticle energy solver	Cubic spline interpolation ($\Delta E = 1$ eV)	Linear spline interpolation ($\Delta E = 0.2$ eV)
Comp. scaling	$\mathcal{O}(N^6)$	$\mathcal{O}(N^4)$
Memory scaling	$\mathcal{O}(N^4)$	$\mathcal{O}(N^4)$
Parameters		
Size of simulation region	R = 12–20 bohr	L= 15–35 bohr
Wavefunction convergence	$h_{\text{grid}} = 0.25$ bohr	E^{ψ}_{cut} = 800–1 000 eV
Max. number of states incl. (N_{tot})	$N_{\text{tot}} \leq 3\,166$	$N_{\text{tot}} \leq 160\,000$
Energy of last state incl. ($E^{\text{last}}_{\text{DFT}}$)	$E^{\text{last}}_{\text{DFT}} \leq 90$ eV	$E^{\text{last}}_{\text{DFT}} = E^{\psi}_{\text{cut}}$
Polarizability basis	Transitions among all states $\leq N_{\text{tot}}$	E^{χ}_{cut} = 200–350 eV N_{freq} = 25–100

their G_0W_0 energies allows us to quantify the error associated with any remaining differences in their numerical implementations. As is explained in this section (and summarized in Table I), this includes not only choice of basis, but also the expressions for integrating the *GW* self-energy, techniques for accelerating the sum-over-states convergence, and methods to solve for the quasiparticle energy. We would like to emphasize that the algorithms employed in conjunction with the real-space and plane-wave implementations are not necessarily imposed by the given basis set; some are chosen because they are the best available option in each software package.

For our combined real-space, transition-space studies, we perform Kohn-Sham DFT calculations with PARSEC[26] and excited-state calculations with RGWBS.[27] Wave functions are defined on a uniform grid within a sphere, and the converged grid spacing is 0.25 bohr. Due to the confined boundary conditions, simulation cells must be sufficiently large to avoid spurious interactions with the boundary walls. We find that the wave functions of the lowest unoccupied molecular orbitals (LUMOs) and all occupied orbitals are converged within 10 meV for simulation cells that have radii of 12 bohr for single-ring molecules, or 14 bohr for double-ringed molecules.

For calculations in the plane-wave basis, we perform ground-state Kohn-Sham DFT calculations using Quantum ESPRESSO[28] and excited-state calculations with BerkeleyGW.[29] Due to the periodic nature of plane-wave basis sets, we need to carefully consider the spurious interactions between repeated supercells. Interactions arising at the *GW* level are removed by numerically truncating the Coulomb potential.[29] For this truncation scheme to be accurate, our simulation cell must be at least twice as big in each Cartesian direction as the region which contains the molecule. We first perform our ground-state DFT calculation on a large unit cell to find the rectangular cuboid which contains a large fraction (99%) of the ground-state charge density. We then double this cuboid in each direction and use it as our unit cell. For such unit cells, however, we also need to account for the almost-rigid shift in the Kohn-Sham eigenvalues due to the spurious interactions between repeated supercells. To accurately determine the energies with respect to the vacuum level, we subtract the electrostatic potential averaged at the surface of the supercell from the mean-field eigenvalues, which leads to a rigid shift of the quasiparticle energies by about 500 meV. We then repeat this procedure on unit cells that are twice and three times as large, with the largest supercells correcting the quasiparticle energies by an amount that ranges from 0 up to 70 meV, depending on the molecule. We obtain final Kohn-Sham eigenvalues via extrapolation and estimate that the corrected eigenvalues for occupied states are accurate to within 10 meV.

For both the real-space and plane-wave frameworks, Equation 1 is represented in terms of quasiparticle quantities:

$$\left[-\frac{1}{2}\nabla^2 + V_H(\mathbf{r}) + V_0(\mathbf{r}) + \Delta\Sigma(E_j^{\mathrm{QP}})\right]\psi_j^{\mathrm{QP}} = E_j^{\mathrm{QP}}\psi_j^{\mathrm{QP}}, \tag{16}$$

where E_j^{QP} is the energy and ψ_j^{QP} is the wave function of quasiparticle in state j. The solution to the above equation requires the evaluation of the *GW* self-energy at E_j^{QP}, which appears on both sides of the above equation but is not known *a priori*. In RGWBS, we explicitly compute $\Sigma(E)$ in an energy range from 10 eV below to 10 eV above each Kohn-Sham eigenvalue (21 points total per eigenvalue, with an energy spacing $\Delta E = 1$ eV), and use a cubic spline interpolation of $\Sigma(E)$ to solve for E_j^{QP}.[27] In BerkeleyGW, we first obtain an approximation $E_j^{\text{QP-HL}}$ to the quasiparticle energy using the Hybertsen-Louie generalized plasmon-pole model[41]. We then evaluate $\Sigma(E)$ on 9 distinct points per eigenvalue in an energy range from 0.8 eV below and above $E_j^{\text{QP-HL}}$, where sucessive evaluations are separated by an energy of $\Delta E = 0.2$ eV. The quasiparticle energy E_j^{QP} is found by performing a piecewise linear interpolation of $\Sigma(\omega)$. The numerical difference between the RGWBS and BerkeleyGW quasiparticle energy solvers due to these differences is expected to be minimal, since the self-energy has a nearly linear slope near the quasiparticle energy.

The expression for the *GW* self-energy Σ at a fixed energy is given by Eq. 7. While the numerical representation of W varies depending on the choice of integration technique (described below), the Green's function in the integrand is expressed as

$$G(\mathbf{r},\mathbf{r}';E) = \sum_n \frac{\varphi_n(\mathbf{r})\varphi_n(\mathbf{r}')}{E - \varepsilon_n + i0^+ \cdot \mathrm{sgn}(\varepsilon_n - \varepsilon_F)}, \tag{17}$$

where φ_n are wave functions, ε_n are energies of the quasiparticle states used to construct G, and ε_F is the Fermi energy. The sum over n converges very slowly with respect to the total number of states, and is one of the primary bottlenecks for *GW* computations.

In the *GW* calculations performed with the RGWBS code, the integral for Σ is split into a bare (Fock) exchange term and a correlation term. The computation of these terms requires a summation over the poles of G (sum over states) as well as the poles of the polarizability.[27] In BerkeleyGW, while calculations still involve a sum over states, the polarizability is stored in the form of dielectric matrix $\varepsilon_{\mathbf{GG}'}$, and its full dynamical effects are computed via the contour deformation technique.[63,64] By eliminating the explicit summation of poles in the polarizability, the formal computational scaling is reduced from $\mathcal{O}(N^6)$ to $\mathcal{O}(N^4)$. Nevertheless, we observe that RGWBS is faster than BerkeleyGW for the molecules in our test set. This is due to a smaller computational prefactor, most likely arising from the efficient spectral representation of the polarizability matrices for small molecules, but becomes prohibitively expensive for extended systems with a continuum of transitions.

Also, in the calculations performed with BerkeleyGW, we find that some quasiparticle solutions lie very close to poles of the self-energy and are thus sensitive to the convergence of the dielectric matrix. These states also tend to move away from these poles during self-consistent *GW* calculations or when starting the G_0W_0 calculations from a different mean-field theory[65]. Therefore, we have not reported the plane-wave G_0W_0 energies of these states. However, these numerical instabilities are not observed in RGWBS calculations, either due to the different frequency representation of the polarizability matrix, or due to differences in the resonant and continuum states, which affect the higher-energy part of the polarizability matrix.

Both RGWBS and BerkeleyGW exploit techniques that improve convergence and reduce the total number of states needed in their sums over states. In RGWBS, we add a correction based on half the static Coulomb-hole screened exchange (COHSEX) to approximate the remainder of a truncated sum over quasiparticle states.[66–68] To accelerate convergence of the sum-over-transitions (poles of the polarizability), we compute the self energy at various levels of convergence (N_{states} satisfying $E_{\text{DFT}}(N_{\text{states}}) = \{20, 30, ..., 90\}$ eV where $E_{\text{DFT}}(N_{\text{states}})$ is the Kohn-Sham DFT eigenvalue of the highest-energy state included in the G and polarizability summations), and obtain a weighted $1/N_{\text{states}}$ extrapolation for a best estimate of numerically converged *GW* self energies.[68–70] The extrapolation produces IPs 50-100 meV larger than the most converged calculation. Note that while we choose the same cutoff of N_{states} for both the calculation of the polarizability and the sum over states, different cutoffs can be applied to these separate summations.

While performing excited-state calculations with BerkeleyGW, we noticed that it is possible to combine several high-energy orbitals having energies about 2% apart from each other into single, unnormalized states for the summation over states. This introduces an error of at most 15 meV, while dramatically speeding up the *GW* calculations. We note that a similar scheme was also recently proposed by Gao *et al.*[71]. Since we include the full Hilbert space in the sum over states, for both the calculation of the self energy and the dielectric matrix, the main convergence parameter for our plane-wave *GW* calculations is the energy cutoff $|\mathbf{G}|^2$ of $\varepsilon_{\mathbf{GG}'}$. We estimate that the quasiparticle energies calculated using a cutoff of 20 Ry for the dielectric matrix are converged to within 90 meV. We also perform *GW* calculations at smaller cutoffs of 15 and 17 Ry and extrapolate the quasiparticle energies as a function of the energy cutoff, which gives accurate extrapolated energies to within approximately 10 meV. For the contour deformation sampling of the polarizability, we find that 15 imaginary frequencies, as well as a set of real frequencies spaced by 250 meV, are sufficient to sample the dielectric matrix and converge most *GW* quasiparticle energies to within 15 meV. For the reported quasiparticle states, we estimate their absolute energies are converged to within 50 meV.

TABLE II. Comparison of EAs in eV, as predicted by real-space DFT (PARSEC) and transition-space G_0W_0 (RGWBS), and plane-wave DFT (Quantum Espresso, denoted by QE) and G_0W_0 (BerkeleyGW). The symmetry of each unoccupied orbital is indicated by σ^*, π^*, or Rydberg $3s$. TTF is in "boat" form, deviating slightly from the planar geometry such that orbitals are not purely σ or π.

	DFT-LDA		G_0W_0@LDA	
Orbital	PARSEC	QE	RGWBS	BerkeleyGW
Benzene				
$1e_{2u}$ (π^*)	1.35	1.36	-0.84	-0.86
$4a_{1g}$ ($3s$)	0.20	0.76	-1.37	-0.25
Naphthalene				
$2b_{1g}$ (π^*)	2.26	2.26	0.38	0.37
$2b_{2g}$ (π^*)	1.51	1.51	-0.31	-0.33
$3b_{3u}$ (π^*)	0.76	0.74	-1.11	-1.11
$10a_g$ ($3s$)	0.29	0.77	-1.05	-0.17
Thiophene				
$4b_1$ (π^*)	1.50	1.51	-0.69	-0.69
$8b_2$ (σ^*)	0.14	0.31	-1.93	-1.33
$2a_2$ (π^*)	-0.19	-0.18	-2.38	-2.34
$12a_1$ ($3s$)	0.11	0.65	-1.34	-0.25
Thiadiazole				
$4b_1$ (π^*)	2.86	2.87	0.62	0.54
$8b_2$ (σ^*)	0.96	0.98	-1.40	-1.34
$2a_2$ (π^*)	0.66	0.67	-1.67	-1.66
$12a_1$ ($3s$)	0.19	0.71	-1.23	-0.23
Benzothiazole				
$7a''$ (π^*)	2.26	2.27	0.34	0.32
$8a''$ (π^*)	1.58	1.59	-0.33	-0.34
$30a'$ (σ^*)	0.91	0.98	-0.99	
$9a''$ (π^*)	0.71		-1.20	
$31a'$ ($3s$)	0.22		-1.06	
TTF				
$17a_1$	1.79	1.80	-0.15	-0.09
$12b_2$	1.60	1.60	-0.32	-0.29
$12a_2$	1.22	1.22	-0.67	-0.59
$15b_1$	0.98	0.99	-0.62	-0.56
$13b_2$	0.69	0.73	-1.23	
$16b_1$	0.46	0.62	-1.26	
$18a_1$ ($3s$)	0.37	0.79	-0.95	-0.17

B. DFT and G_0W_0 comparison

For the real-space and plane-wave basis sets, we match orbitals according to their wave function symmetry and find that the mean-field DFT-LDA energies are in good agreement with each other. The two frameworks predict eigenvalues that deviate no more than 12 meV for our benchmark test set, which includes the LUMOs (which

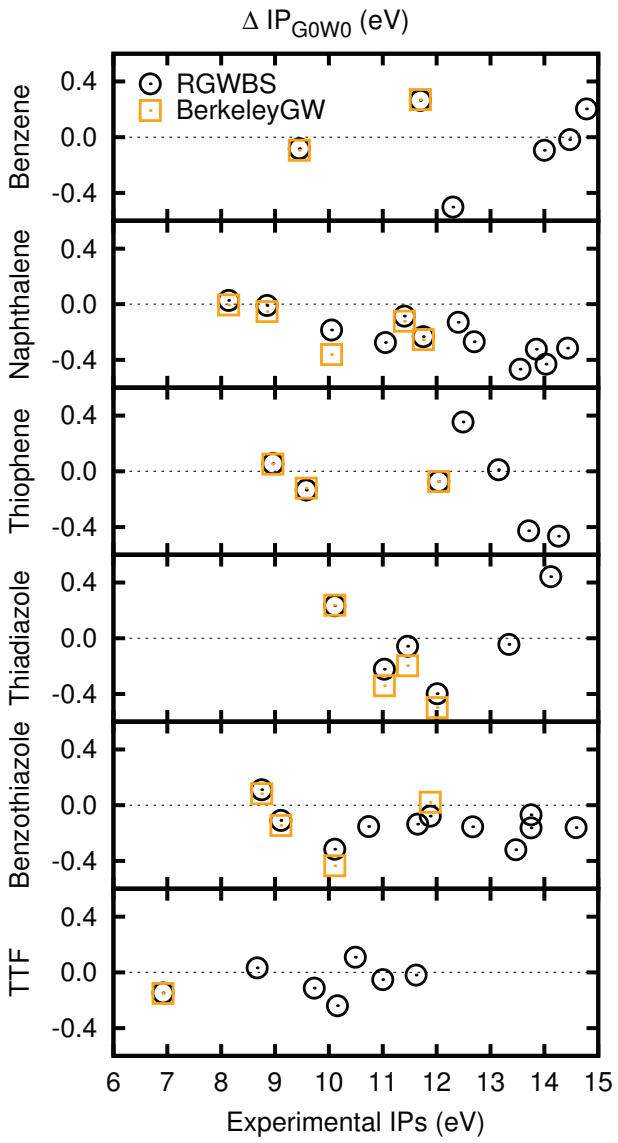

FIG. 1. Error of the IPs of all molecules predicted via G_0W_0, relative to experiment.[72–77] Black circles are computed using RGWBS (real-space framework) and orange squares are computed using BerkeleyGW (plane-wave framework).

are bound by DFT-LDA) and occupied orbitals with experimental IPs that are less than 15 eV. We also assess additional low-lying unoccupied orbitals that DFT-LDA predicts to be bound (Table II). For the localized unoccupied orbitals (σ^* and π^*), energy differences are typically less than 20 meV; however, diffuse orbitals with Rydberg ($3s$) character have eigenvalues that may differ by more than 500 meV between the two frameworks. We also observe that certain unbound orbitals, such as the $2a_2$ orbital of thiophene, are also highly localized.

At the G_0W_0 level of theory, differences between energies remain minimal: frontier (highest occupied and lowest unoccupied) orbitals differ by no more than 80 meV, and IPs are in good agreement (Figure 1), with only five IPs differing by more than 100 meV in the entire test set despite the different basis sets and numerical techniques. For the energies corresponding to adding an electron to low-lying unoccupied orbitals, those that are converged with respect to simulation cell size at the DFT-LDA level also have comparable G_0W_0 energies (Table II). However, the energies of those affected by the boundary conditions diverge even more at the G_0W_0 level. At an extreme, G_0W_0 predictions of some EAs for Rydberg s orbitals differ by more than 1 eV.

These benchmarks of plane-wave GW calculation implemented in BerkeleyGW, compared to real-space GW implemented in RGWBS, confirm that numerical errors for GW predictions are minimal in both frameworks, as long as the orbitals studied are unaffected by boundary conditions at the DFT level of theory. With this validation, we expect that GW energies are numerically converged to within 100 meV for localized orbitals and proceed with a quantitative assessment of excitations between such orbitals; we qualitatively study trends for excited state properties involving continuum or Rydberg states.

C. Additional computational details

In the remainder of this work, we examine how the computed vertical IPs, EAs, and singlet excitation energies are affected by self-consistency and the choice of vertex function in GW using the RGWBS code. While we focus on trends for the predicted accuracy of each method, tables containing computed energies and symmetries of quasiparticles and singlet excitations are available in our Supplemental Material.

For any calculation including Γ_{LDA}, we maintain a consistent level of approximation. Specifically, LDA exchange-correlation contributes to both the screened Coulomb interaction and the self energy for $G_0W_0\Gamma_{\mathrm{LDA}}$ and QS$GW\Gamma_{\mathrm{LDA}}$ calculations, and the BSE kernel associated with one-particle Green's functions that use Γ_{LDA} also has a LDA-derived term.[27]

QSGW and QS$GW\Gamma_{\mathrm{LDA}}$ calculations include a basis of quasiparticles up to DFT energies of at least 10 eV ($\sim$ 90 states for the molecules considered). Calculations are performed summing over states up to DFT energies of 40 eV, and the difference in energy compared to the perturbative calculation (G_0W_0 or $G_0W_0\Gamma_{\mathrm{LDA}}$ at the 40 eV sum-over-states cutoff) is added to the best-estimate perturbative extrapolation to produce best-estimate QS quasiparticle energies. QS quasiparticles of most molecules are optimized until energy differences are less than 10 meV, except for benzothiazole and TTF, which are only optimized to 80 and 50 meV, respectively.

The TDLDA and BSE calculations are converged within 100 meV when summing over all orbitals up to Kohn-Sham DFT energies of 20 eV. For both TDLDA and BSE calculations, we do not use the Tamm-Dancoff approximation.

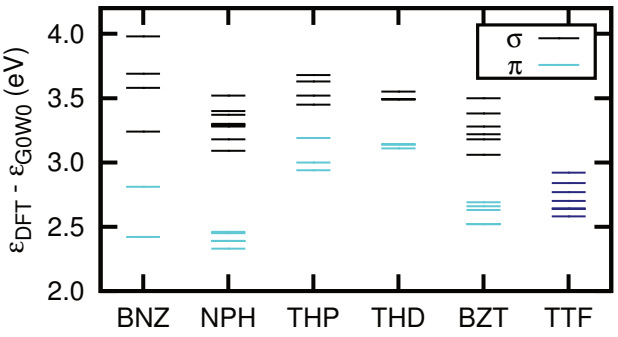

FIG. 2. (Color online) *GW* self-energy corrections to Kohn-Sham DFT eigenvalues for benzene (BNZ), naphthalene (NPH), thiophene (THP), 1,2,5-thiadiazole (THD), benzothiazole (BZT), and TTF. The shifts for orbitals with π character are in black, and shifts for all other orbitals (σ or lone pair character) are shown in cyan. The "boat" form of TTF is not aromatic and its self-energy corrections (dark blue) cannot be partitioned into two groups as in the other molecules.

IV. *GW* AND BSE BENCHMARKS

A. Vertical IPs and EAs

The G_0W_0 IPs shown earlier in Figure 1 indicate good agreement with experimental measurements. We now examine whether *GW* calculations are affected by the physical character of the orbitals. In our aromatic molecule test set, benzene, naphthalene, thiophene, 1,2,5-thiadiazole, and benzothiazole all have orbitals with purely σ or π character. However, for TTF, we study the "boat" form, whose small deformation from the aromatic planar geometry prevents the existence of delocalized π orbitals.

On this test set, we see no correlation between the errors of G_0W_0-predicted IPs and the type of the orbitals. In contrast, we do observe differences in the magnitude of the *GW* correction, as has also been noted in some previous studies of molecules.[6,10] (Similar observations of orbital character dependence of the self-energy corrections were also found in condensed matter systems.[41]) The self-energy corrections obtained from G_0W_0 and starting from DFT-LDA are shown in Fig. 2. For aromatic molecules, corrections for σ (including lone-pair) orbitals are all larger than corrections for π orbitals, while TTF does not exhibit any partitioning. The difference between *GW* corrections for occupied π and σ orbitals persists across the variants of *GW* in our study, although we note that similar trends do not apply to unoccupied σ^* and π^* orbitals. This reflects a systematic error of the DFT-LDA mean-field starting point: while DFT-LDA underbinds all occupied orbitals, it is more accurate when modeling the delocalized π orbitals compared to the localized σ orbitals in aromatic molecules. In addition, the relatively large range of *GW* self-energy corrections result in rearrangements of the orbital energy orderings when

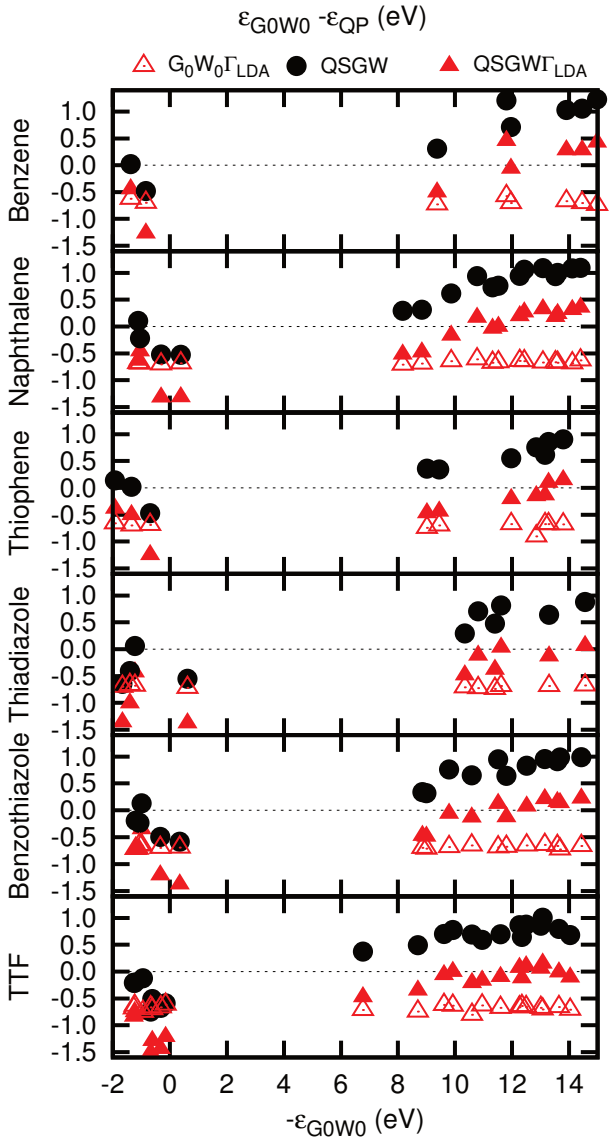

FIG. 3. (Color online) Shift of quasiparticles energies from predictions at G_0W_0, for *GW* variants including self-consistency and vertex corrections.

going from DFT-LDA to *GW*. The resulting orderings are consistent with literature. Perturbative *GW* does improperly predict that the $3e_{2u}$ orbital in benzene is more bound than the $1a_{2u}$ orbital, but this is corrected upon application of self-consistency. Apart from this example and some near-degenerate IPs, there are no changes in *GW*-predicted energy orderings due to $\Gamma_{\rm LDA}$ and quasiparticle self-consistency.

The overall effects of $\Gamma_{\rm LDA}$ and quasiparticle self-consistency, in relation to conventional G_0W_0, are shown in Fig. 3. Compared to G_0W_0 IPs, $G_0W_0\Gamma_{\rm LDA}$ predictions are consistently shifted downward by 0.69 eV (standard deviation 0.05 eV). The IPs predicted by QS$GW\Gamma_{\rm LDA}$ also remain nearly a constant shift below those predicted by standard QSGW, with a nominal in-

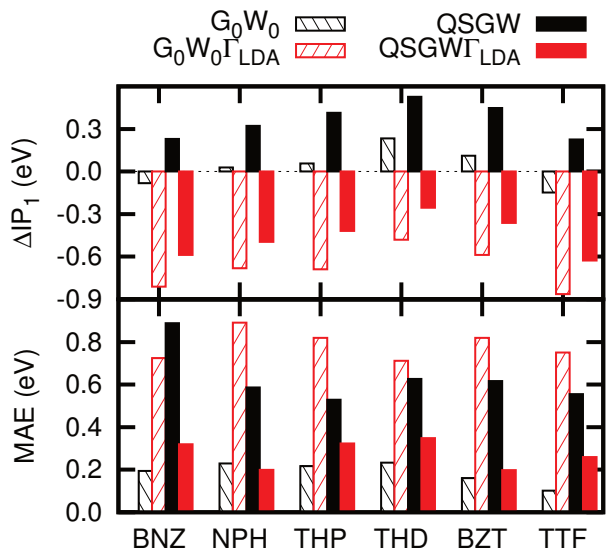

FIG. 4. (Color online) Error for the first IP (top) and the mean absolute error of orbitals with IPs up to 15 eV (bottom), relative to experiment for each molecule.[72–77]

crease of the energy difference to 0.79 eV (standard deviation 0.04 eV). However, quasiparticle self-consistency, both with and without $\Gamma_{\rm LDA}$, makes the occupied orbitals more bound compared to the perturbative calculations. While the first IP is only slightly shifted upward, deeper orbitals exhibit a greater shift. The separate effects of the nearly-constant shift of eigenvalues after applying $\Gamma_{\rm LDA}$ and the opening of the GW gap upon self-consistency agree with previous benchmarks mentioned in Sec. II A. Our results also demonstrate that $\Gamma_{\rm LDA}$ and self-consistency still behave with the same trends when combined in QS$GW\Gamma_{\rm LDA}$ as they do separately.

For the EAs, analogous trends exist for the shifts from G_0W_0 with $\Gamma_{\rm LDA}$ and self consistency. $G_0W_0\Gamma_{\rm LDA}$ calculations give EAs lower than G_0W_0 by 0.68 eV (standard deviation 0.04 eV). Because these shifts are nearly identical to those of the IPs, the fundamental gap is practically unchanged going from G_0W_0 to $G_0W_0\Gamma_{\rm LDA}$. The LUMOs computed via QS$GW\Gamma_{\rm LDA}$ are on average 0.77 eV lower than QSGW (standard deviation 0.07 eV), again a comparable shift to the occupied states that results in an essentially unchanged fundamental gap whether or not the vertex correction is applied at the self-consistent level. In constrast, quasiparticle self-consistency increases the fundamental gap by 0.8-0.9 eV, since in both QSGW and QS$GW\Gamma_{\rm LDA}$, the EAs move in the opposite direction from IPs and become more negative (less bound) compared to perturbative results.

Experimental measurements exist for IPs up to 15 eV in most of the molecules, and we find that of the various types of GW benchmarked here, G_0W_0 predictions of IPs (corresponding to hole-creation quasiparticle energies) still give the best agreement with experimental measurements, all lying within 0.6 eV of measured values with a mean absolute error less than 0.3 eV (Fig. 1 and Fig. 4). Predictions from $G_0W_0\Gamma_{\rm LDA}$ are too low, consistent with a benchmark of single atoms.[48] However, upon applying quasiparticle self-consistency, the increased binding of the quasiparticle energies results in a switching of the trends: while the QSGW IPs' increase from perburbative values result in a decrease in accuracy, the increase in QS$GW\Gamma_{\rm LDA}$ IPs improves agreement with experiment. Our results concerning self consistency stand in contrast to past calculations using atom-centered basis sets, which suggest that eigenvalue, QS, and fully self-consistent GW can improve spectral properties for molecules.[2–5,10,13,15,17,22,24,52,55] At the same time, the systematic deterioration in accuracy in our QSGW also differs from a plane-wave implementation of self-consistent GW, which does not show a clear trend for increasing or decreasing accuracy with the same DFT-LDA starting point.[19] We observe that for self-consistent GW, numerical considerations such as the choice of a quasiparticle basis for self-consistency, as well as the basis set chosen to represent wave functions, must be better understood before a consensus can be reached on the theoretical accuracy of self-consistent GW for molecules.

There are few measurements available for EAs; those for benzene and naphthalene are reported in Table III together with our GW predictions. For these EAs, $G_0W_0\Gamma_{\rm LDA}$ and QSGW are closest in value. EAs from $G_0W_0\Gamma_{\rm LDA}$ are in particularly good agreement with CCSD(T), but both are too negative relative to experiment. It is unclear whether these differences are due to the difficulties in experimental measurement, or an inaccurate representation of the unoccupied orbitals in the calculations. In particular, the CCSD(T) performs the higher-order corrections on a limited basis set, which may numerically bind the wave functions, and similarly, our perturbative calculations use a DFT-LDA electronic structure, a theory which over-binds the unoccupied orbitals. Nevertheless, comparison of $G_0W_0\Gamma_{\rm LDA}$ and QSGW allows us to predict that the first EA for nearly all the aromatic molecules in our test set are negative; only 1,2,5-thiadiazole might have a positive EA.

Altogether, we see that no single variant of GW studied here is most accurate for both IPs and EAs. For perturbative calculations, G_0W_0 is more accurate for IPs, and $G_0W_0\Gamma_{\rm LDA}$ is more accurate for EAs, while among self-consistent calculations (which reduce or eliminate starting point dependence), QS$GW\Gamma_{\rm LDA}$ is more accurate for IPs, and QSGW is more accurate for EAs. This illustrates, with real molecules, an earlier prediction derived from model systems: while a two-point DFT-derived vertex can alleviate self-screening errors felt by occupied orbitals, only a three-point vertex can be expected to treat both occupied and unoccupied orbitals accurately.[46] Nevertheless, we also note that the fundamental gaps of benzene and naphthalene computed using QSGW (11.01 and 8.61 eV, respectively) and QS$GW\Gamma_{\rm LDA}$ (10.98 and 8.57 eV) are nearly identical to fundamental gaps determined from experimental IPs and

TABLE III. First EA in eV with comparison to electron transmission spectroscopy (ETS) measurements[78] and CCSD(T)[79] calculations when available.

Molecule	Orbital	ETS	CCSD(T)	G_0W_0	$G_0W_0\Gamma_{\mathrm{LDA}}$	QSGW	QS$GW\Gamma_{\mathrm{LDA}}$
Benzene	$1e_{2u}$ ($\pi*$)	-1.12	-1.526	-0.84	-1.55	-1.33	-2.12
Naphthalene	$2b_{1g}$ (π^*)	-0.19	-0.477	0.38	-0.30	-0.15	-0.93
Thiophene	$4b_1$ (π^*)			-0.69	-1.38	-1.17	-1.94
1,2,5-Thiadiazole	$4b_1$ (π^*)			0.62	-0.10	0.07	-0.76
Benzothiazole	$7a''$ (π^*)			0.34	-0.35	-0.24	-1.04
TTF	$17a_1$			-0.15	-0.76	-0.74	-1.36

CCSD(T) EAs (10.98 and 8.62 eV).

Our benchmarks show a cancellation between the effects of vertex corrections and GW self-consistency as reported in earlier work,[35,36,38] except here the cancellation only exists for the IPs. For EAs, on the other hand, we see that the vertex and self-consistency effects are still roughly the same magnitude, but they shift in the same direction from G_0W_0 predictions, such that QS$GW\Gamma_{\mathrm{LDA}}$ compounds their effects instead of canceling them out. Benchmarks on a larger and more diverse test sets may be able to assess whether the comparable magnitudes of self-consistency and vertex corrections are coincidental, or if they can be attributed to physical properties of aromatic or *sp*-bonded molecules. For now, we simply observe that for the molecules studied, G_0W_0 gives IPs closest to experiment, and $G_0W_0\Gamma_{\mathrm{LDA}}$ gives EAs closest to best available theoretical values at a relatively cheap computational cost.

B. Vertical singlet excitation energies

Singlet excitation energies may be obtained either by TDLDA or by applying the BSE to GW electronic structures described in the previous section. In addition to applying the BSE to perturbative GW and self-consistent GW, with and without Γ_{LDA}, we also apply the BSE to a mixed set of GW quasiparticles, where occupied orbitals are associated with G_0W_0 quasiparticle energies, unoccupied orbitals have $G_0W_0\Gamma_{\mathrm{LDA}}$ quasiparticle energies, and the screened interaction is computed using LDA quantities without vertex contributions. The quasiparticle wave functions in this case are given by the DFT wave functions. This calculation, which we denote as mixed GW-BSE, is motivated by the observation in the previous section that G_0W_0 energies have the best agreement with experimental values for IPs, while $G_0W_0\Gamma_{\mathrm{LDA}}$ energies are better for EAs.

In Fig. 5, we show the first-principles absorption spectra up to excitations of 8 eV for each of the molecules in our test set. The TDLDA spectra in the top row are computed using two simulation cell sizes to illustrate the convergence of the spectra with the spatial range of the cell. While the lowest-energy excitations are in agreement, deviations are observed as excitation energy increases. The remaining rows illustrate the spectra for each variant of GW-BSE. Overall, the peaks of TDLDA, self-consistent GW-BSE and mixed GW-BSE are mostly aligned, while results from solving the BSE using quasiparticle quantities from perturbative G_0W_0 and $G_0W_0\Gamma_{\mathrm{LDA}}$ exhibit a red-shift of all peaks compared to the other spectra.

The singlet excitations obtained in GW-BSE and TDLDA calculations involve excitations to two types of unoccupied orbitals: unoccupied valence orbitals (molecular orbitals constructed from atomic orbitals with the same principal quantum number as the atoms' valence orbitals) and Rydberg orbitals (molecular orbitals which have contributions from atomic orbitals with principal quantum number higher than the atoms' valence orbitals). Singlet excitations with transitions primarily into the localized valence orbitals are termed valence excitations, and those with transitions primarily into the diffuse Rydberg orbitals are termed Rydberg excitations. We discuss the accuracy of GW-BSE and TDLDA calculations for each type of excitation separately.

Our detailed comparison of GW-BSE predictions of valence excitations, including singlet states that are symmetry-forbidden in linear optical processes, is shown in the top panel of Fig. 6. All calculations are presented as the difference from mixed GW-BSE predictions. The choice of vertex is found to barely change excitation energies, with the inclusion of Γ_{LDA} increasing energies by an average of 0.09 eV for perturbative GW-BSE, and by an even smaller average increase of 0.02 eV for QSGW-BSE. As mentioned in the previous section, the energy differences between quasiparticles (both holes and quasielectrons) from G_0W_0 and $G_0W_0\Gamma_{\mathrm{LDA}}$ essentially amounts to a rigid shift, and energy differences between quasiparticle levels remains unchanged. These small differences in transition energies instead mostly arise from the inclusion of Γ_{LDA} in the BSE equation itself.

On the other hand, self-consistency in GW widens both the fundamental and optical gap to significantly increase excitation energies from the perturbative GW-BSE results. QSGW-BSE has an average 0.91 eV increase of singlet excitation energies over G_0W_0-BSE, and QS$GW\Gamma_{\mathrm{LDA}}$-BSE has an average 0.84 eV increase compared to $G_0W_0\Gamma_{\mathrm{LDA}}$-BSE. Mixed GW-BSE also has an optical gap larger than perturbative GW-BSE calculations by $\sim$0.6-0.7 eV, since by associating G_0W_0 energies with occupied orbitals and $G_0W_0\Gamma_{\mathrm{LDA}}$ energies with unoccupied orbitals, the fundamental gap is increased by

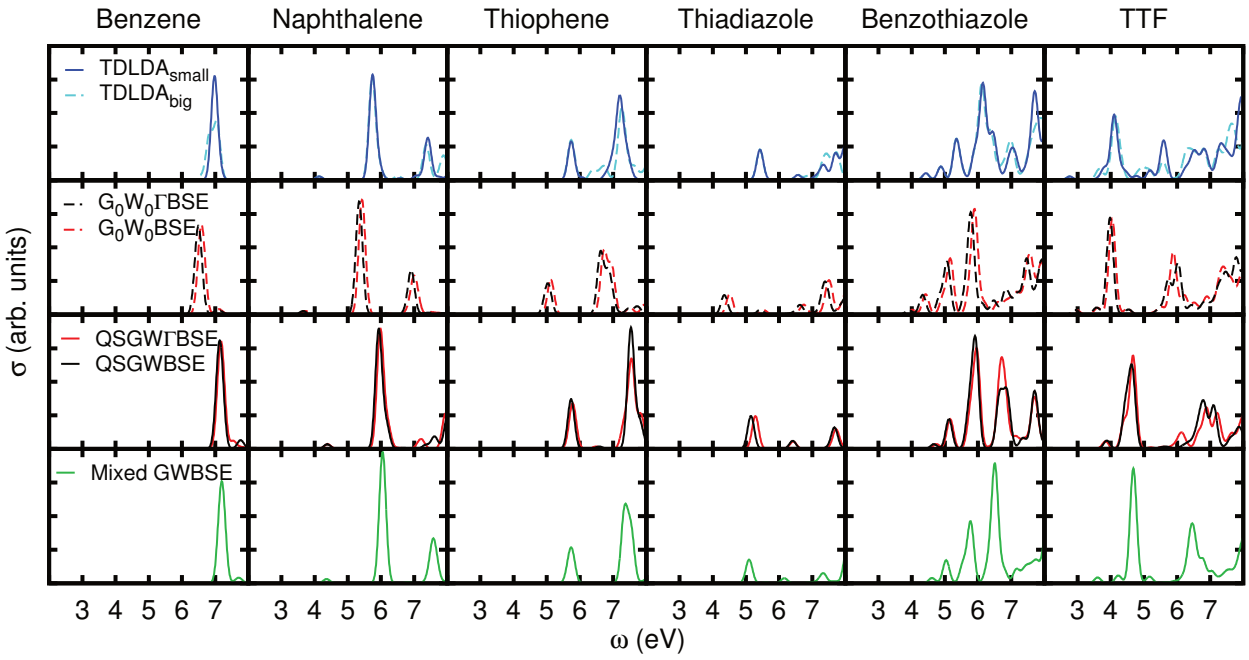

FIG. 5. (Color online) The absorption cross section for each of the molecules convoluted with a Gaussian broadening of 0.1 eV, as predicted by various levels of theory. The TDLDA$_{\rm big}$ calculations are performed in simulation cells with radii of 20 bohr, while TDLDA$_{\rm small}$ simulation cells have radii that are either 12 bohr (for benzene, thiophene, and 1,2,5-thiadiazole) or 14 bohr (for naphthalene, benzothiazole, and TTF). *GW*-BSE calculations are performed in the smaller simulation cells.

∼0.7 eV.

Comparison of our results for valence singlet excitation energies to best previous theoretical results for benzene, naphthalene, thiophene and 1,2,5-thiadiazole are shown in the bottom panel of Fig. 6 and in the left panel of Fig. 7. For benzene, naphthalene, and thiophene, our self-consistent and mixed *GW*-BSE calculations have fairly good agreement best previous theoretical values, which are computed including contributions from singles, doubles, and triples excitations.[80–82] The mean absolute difference across these three molecules is 0.78 eV for G_0W_0-BSE, 0.68 eV for $G_0W_0\Gamma_{\rm LDA}$, 0.14 for mixed *GW*-BSE, 0.25 for QS*GW*-BSE, 0.24 for QS*GW*$\Gamma_{\rm LDA}$-BSE, and 0.25 for TDLDA. For 1,2,5-thiadiazole, the cited calculation only include singles and doubles excitations,[83] and the mean absolute difference is 1.26 eV for G_0W_0-BSE, 1.14 eV for $G_0W_0\Gamma_{\rm LDA}$, 0.58 eV for mixed *GW*-BSE, 0.33 eV for QS*GW*-BSE, 0.29 for *GW*$\Gamma_{\rm LDA}$-BSE, and 0.61 for TDLDA. BSE calculations that follow perturbative *GW* calculations are all smaller than the excitation energies from the best previous theoretical calculations. For benzene, naphthalene, and thiophene, the mean signed difference is -0.7 to -0.8 eV for G_0W_0-BSE and $G_0W_0\Gamma_{\rm LDA}$-BSE. This is reduced to a mean signed difference of approximately -0.1 eV for mixed *GW*-BSE. For QS*GW*-BSE and QS*GW*$\Gamma_{\rm LDA}$-BSE, the mean signed difference is negative for benzene, but positive for naphthalene and thiophene.

Finally, we present the comparison between previous theoretical best estimates and our results for Rydberg excitations in Fig. 7. However, we caution that simulation cells used for our *GW*-BSE calculations confine the diffuse Rydberg wave functions and we thus only discuss qualitative trends for these excitations. To account for the presence of confining walls, we make the assumption that energy increase due to confinement remains constant across all levels of theory, and plot *GW*-BSE energies from calculations in a small cell, shifted downward by the difference between TDLDA calculations using a large simulation cell (radius 20 bohr) and TDLDA calculations in a small cell used by *GW*-BSE. Our perturbative *GW*-BSE and TDLDA calculations predict comparable Rydberg excitation energies (difference of -0.01 to 0.32 eV), in contrast to the red-shift observed for perturbative *GW*-BSE predictions of valence excitations. Both perturbative *GW*-BSE and TDLDA underestimate the best previous theoretical values. Application of quasiparticle self-consistency or the mixed *GW*-BSE technique increases excitation energies by approximately 0.4 or 0.6 eV, respectively, which improves agreement with past results.

Our calculations confirm that TDLDA predictions for localized valence excitations within *sp*-bonded molecules are in good agreement with higher-level quantum chemistry calculations, but the LDA functional's incorrect asymptotic behavior results in a deterioration of its accuracy when long-range interactions become important, as in Rydberg excitations.[84,85] Within TDDFT, functionals

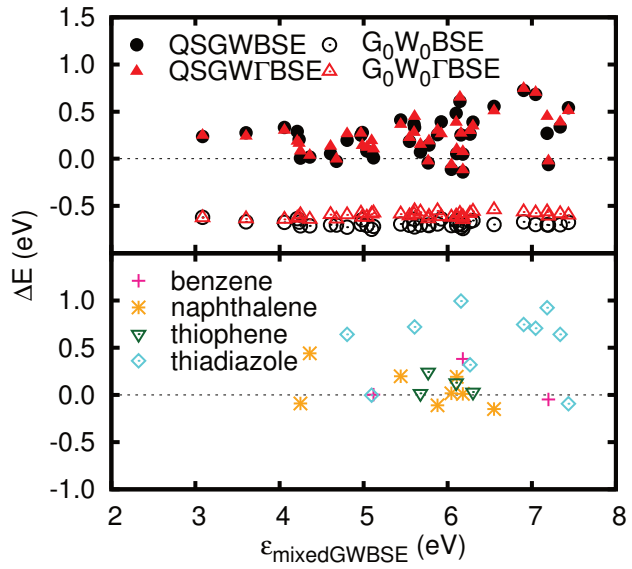

FIG. 6. (Color online) The top panel compares GW-BSE calculations for valence (localized) excitations, taking the mixed GW-BSE predictions as reference. The bottom panel again uses the mixed GW-BSE results as reference and illustrates the deviations from the best available theoretical values in literature.[80–83]

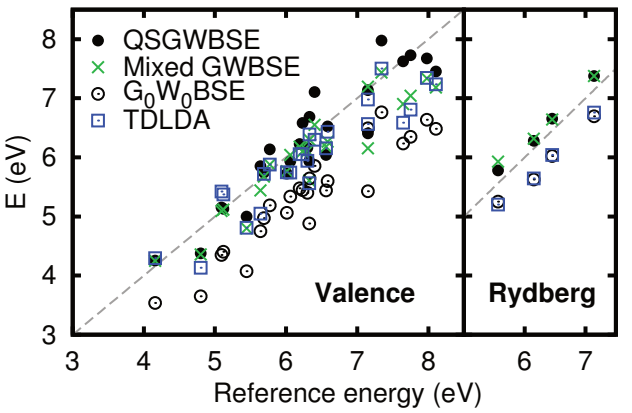

FIG. 7. (Color online) The deviation of various first-principles methods relative to previous best available theoretical values (labeled as reference) for the vertical valence (left) and Rydberg (right) excitation energies.[80–83]

that better account for exchange and correlation interactions must be used to produce good optical spectra for molecules.[86–88] The GW-BSE framework, on the other hand, treats Rydberg and valence excitations on equal footing. We see that the relatively inaccurate DFT-LDA mean-field starting point is already sufficient to initialize (self-consistent or mixed) GW-BSE calculations that describe of neutral excitations in aromatic molecules with improved accuracy, whether the excitations have valence or Rydberg character.

V. CONCLUSIONS

In this work, we perform GW computations to investigate the many-body perturbation-theory predictions of excited-state properties in aromatic molecules. Our combined real-space and transition-space implementation is validated by comparison to computations on a plane-wave basis set, with all calculations explicitly including the dynamic effects of the polarizability matrix. Given the myriad differences between numerical algorithms and convergence techniques, we find that G_0W_0 energies obtained from RGWBS (real- and transition-space) and BerkeleyGW (plane-wave) are in remarkable agreement, with nearly all energies agreeing to within 0.1 eV for occupied and low-lying unoccupied orbitals (that is, for the single-particle excitation energies).

The uniform grid used in our real-space computations allows the simulation of orbitals with localized, diffuse, or even continuum character. We examine the accuracy of the IPs, EAs, and the GW-BSE excitation energies for valence singlet excitations, and study the trends of Rydberg excitations within GW-BSE. Our ability to simulate Rydberg excitations is limited by the computational cost, but to our knowledge, this is the first attempt to even qualitatively assess the accuracy of Rydberg excitation energies within GW-BSE. Our simulations show that self-consistent GW-BSE predicts larger Rydberg excitation energies than TDLDA, which results in better agreement with previous best-estimate values.

The spectral representation of the polarizability in our transition-space calculations results in an efficient yet accurate calculation of GW self energies. We therefore use this framework to analyze the performance of variants of GW, including the effects of Γ_{LDA} and quasiparticle self-consistency, both alone and combined. We see that alone, Γ_{LDA} leaves energy level spacings nearly the same, but that all IPs and EAs are shifted up by $\sim$0.7 eV to become less bound for the molecules considered. Quasiparticle self-consistency applied to conventional GW opens the fundamental gap for all molecules, increasing both the hole and quasielectron energies relative to the results of perturbative GW. In the combined QS$GW\Gamma_{\mathrm{LDA}}$, the overall change in self-energies is essentially the two independent corrections combined; we do not observe higher-order interactions of quasiparticle self-consistency and Γ_{LDA}. Nevertheless, we note that the Γ_{LDA} corrections and self-consistency effects are of similar magnitude on our test set. This results in a cancellation of effects for IPs, and a compounding of effects for EAs, such that G_0W_0 and QS$GW\Gamma_{\mathrm{LDA}}$ are closer to previous best-estimate values for occupied orbitals, and $G_0W_0\Gamma_{\mathrm{LDA}}$ and QSGW are better for unoccupied orbitals. Our results show again that a three-point vertex is needed to improve accuracy beyond conventional GW for modeling both occupied (electron removal) and unoccupied (electron injection) states in molecules.

Our results on valence singlet excitations, with and without Γ_{LDA} and self-consistency, reflect the influence

of the quasiparticle input on the resulting BSE values. Since $\Gamma_{\rm LDA}$ leaves relative quasiparticle energies differences unchanged, the addition of this vertex to GW-BSE calculations typically changes the predicted energies by less than 0.1 eV. The underestimated fundamental gap in perturbative GW results in underestimated excitations energies from perturbative GW-BSE, while the increased fundamental gap of self-consistent GW is reflected in the corresponding increase in the excitation energies for self-consistent GW-BSE. For self-consistent GW-BSE, mean absolute differences from best available previous theoretical values are no larger than 0.33 eV for all molecules. We also construct mixed GW quasiparticles whose IPs and EAs are closest to the best available previous theoretical values, by using DFT-LDA wave functions, G_0W_0 energies for occupied orbitals, and $G_0W_0\Gamma_{\rm LDA}$ energies for unoccupied orbitals; the singlet excitation energies of mixed GW-BSE are comparable to those from self-consistent GW-BSE.

By focusing on the simple DFT-LDA starting point, this work complements other recent publications that seek to improve agreement between G_0W_0 calculations and experimental measurements by using alternate mean-field starting points.[8,11,21] Moving beyond the popular G_0W_0 method, we obtain a better theoretical understanding of the strengths and weaknesses of the perturbative and self-consistent GW approximations, the vertex function, and the BSE. Our work demonstrates the capabilities of a combined real-space and transition-space GW-BSE implementation, as these methods become ever more relevant in the study of molecules, clusters, and other finite systems.

ACKNOWLEDGMENTS

L.H. and S.Ö. would like to thank the U.S. Department of Energy Grant No. DE-FG02-09ER16072 for support. Part of this research (F.H.J. and S.G.L) was supported by the Scientific Discovery through Advanced Computing (SciDAC) Program on Excited State Phenomena in Energy Materials funded by the U. S. Department of Energy, Office of Basic Energy Sciences and of Advanced Scientific Computing Research, under Contract No. DE-AC02-05CH11231 at the Lawrence Berkeley National Laboratory which provided for algorithm and code developments and simulations, and by the National Science Foundation under grant DMR-1508412 which provided for basic theoretical analyses. J.S.C. and J.R.C. also acknowledge support provided by the SciDAC program funded by U.S. Department of Energy, Office of Science, Advanced Scientific Computing Research and Basic Energy Sciences under award number DE-SC0008877. All authors used resources at the National Energy Research Scientific Computing Center, a DOE Office of Science User Facility supported by the Office of Science of the U.S. Department of Energy under Contract No. DE-AC02-05CH11231.

* linda.hung@nist.gov
† ogut@uic.edu

[1] Y. Ma, M. Rohlfing, and C. Molteni, J. Chem. Theory Comput. **6**, 257 (2010).
[2] C. Rostgaard, K. W. Jacobsen, and K. S. Thygesen, Phys. Rev. B **81**, 085103 (2010).
[3] X. Blase, C. Attaccalite, and V. Olevano, Phys. Rev. B **83**, 115103 (2011).
[4] S.-H. Ke, Phys. Rev. B **84**, 205415 (2011).
[5] C. Faber, C. Attaccalite, V. Olevano, E. Runge, and X. Blase, Phys. Rev. B **83**, 115123 (2011).
[6] X. Qian, P. Umari, and N. Marzari, Phys. Rev. B **84**, 075103 (2011).
[7] X. Blase and C. Attaccalite, Appl. Phys. Lett. **99**, 171909 (2011).
[8] X. Ren, P. Rinke, V. Blum, J. Wieferink, A. Tkatchenko, A. Sanfilippo, K. Reuter, and M. Scheffler, New J. Phys. **14**, 053020 (2012).
[9] B. Baumeier, D. Andrienko, Y. Ma, and M. Rohlfing, J. Chem. Theory Comput. **8**, 997 (2012).
[10] N. Marom, F. Caruso, X. Ren, O. T. Hofmann, T. Körzdörfer, J. R. Chelikowsky, A. Rubio, M. Scheffler, and P. Rinke, Phys. Rev. B **86**, 245127 (2012).
[11] F. Bruneval and M. A. L. Marques, J. Chem. Theory Comput. **9**, 324 (2013).
[12] T. A. Pham, H.-V. Nguyen, D. Rocca, and G. Galli, Phys. Rev. B **87**, 155148 (2013).
[13] F. Caruso, P. Rinke, X. Ren, A. Rubio, and M. Scheffler, Phys. Rev. B **88**, 075105 (2013).
[14] V. Atalla, M. Yoon, F. Caruso, P. Rinke, and M. Scheffler, Phys. Rev. B **88**, 165122 (2013).
[15] P. Koval, D. Foerster, and D. Sánchez-Portal, Phys. Rev. B **89**, 155417 (2014).
[16] P. Boulanger, D. Jacquemin, I. Duchemin, and X. Blase, J. Chem. Theory Comput. **10**, 1212 (2014).
[17] S. Körbel, P. Boulanger, I. Duchemin, X. Blase, M. A. L. Marques, and S. Botti, J. Chem. Theory Comput. **10**, 3934 (2014).
[18] D. Hirose, Y. Noguchi, and O. Sugino, Phys. Rev. B **91**, 205111 (2015).
[19] L.-W. Wang, Phys. Rev. B **91**, 125135 (2015).
[20] K. Krause, M. E. Harding, and W. Klopper, Mol. Phys. **113**, 1952 (2015).
[21] F. Bruneval, S. M. Hamed, and J. B. Neaton, J. Chem. Phys. **142**, 244101 (2015).
[22] D. Jacquemin, I. Duchemin, and X. Blase, J. Chem. Theory Comput. **11**, 3290 (2015).
[23] M. J. van Setten, F. Caruso, S. Sharifzadeh, X. Ren, M. Scheffler, F. Liu, J. Lischner, L. Lin, J. R. Deslippe, S. G. Louie, C. Yang, F. Weigend, J. B. Neaton, F. Evers, and P. Rinke, J. Chem. Theory Comput. **11**, 5665 (2015).
[24] J. W. Knight, X. Wang, L. Gallandi, O. Dolgounitcheva, X. Ren, J. V. Ortiz, P. Rinke, T. Körzdörfer, and N. Marom, J. Chem. Theory Comput. **12**, 615 (2016).

[25] L. Hedin, Phys. Rev. **139**, A796 (1965).
[26] L. Kronik, A. Makmal, M. L. Tiago, M. M. G. Alemany, M. Jain, X. Huang, Y. Saad, and J. R. Chelikowsky, Phys. Status Solidi B **243**, 1063 (2006).
[27] M. L. Tiago and J. R. Chelikowsky, Phys. Rev. B **73**, 205334 (2006).
[28] P. Giannozzi, S. Baroni, N. Bonini, M. Calandra, R. Car, C. Cavazzoni, D. Ceresoli, G. L. Chiarotti, M. Cococcioni, I. Dabo, A. Dal Corso, S. de Gironcoli, S. Fabris, G. Fratesi, R. Gebauer, U. Gerstmann, C. Gougoussis, A. Kokalj, M. Lazzeri, L. Martin-Samos, N. Marzari, F. Mauri, R. Mazzarello, S. Paolini, A. Pasquarello, L. Paulatto, C. Sbraccia, S. Scandolo, G. Sclauzero, A. P. Seitsonen, A. Smogunov, P. Umari, and R. M. Wentzcovitch, J. Phys.: Condens. Matter **21**, 395502 (2009).
[29] J. Deslippe, G. Samsonidze, D. A. Strubbe, M. Jain, M. L. Cohen, and S. G. Louie, Comput. Phys. Commun. **183**, 1269 (2012).
[30] S. V. Faleev, M. van Schilfgaarde, and T. Kotani, Phys. Rev. Lett. **93**, 126406 (2004); M. van Schilfgaarde, T. Kotani, and S. Faleev, *ibid.* **96**, 226402 (2006).
[31] R. Del Sole, L. Reining, and R. W. Godby, Phys. Rev. B **49**, 8024 (1994).
[32] P. Minnhagen, J. Phys. C **7**, 3013 (1974).
[33] G. D. Mahan and B. E. Sernelius, Phys. Rev. Lett. **62**, 2718 (1989).
[34] P. A. Bobbert and W. van Haeringen, Phys. Rev. B **49**, 10326 (1994).
[35] H. J. de Groot, R. T. M. Ummels, P. A. Bobbert, and W. van Haeringen, Phys. Rev. B **54**, 2374 (1996).
[36] E. L. Shirley, Phys. Rev. B **54**, 7758 (1996).
[37] A. Schindlmayr and R. W. Godby, Phys. Rev. Lett. **80**, 1702 (1998).
[38] R. T. M. Ummels, P. A. Bobbert, and W. van Haeringen, Phys. Rev. B **57**, 11962 (1998).
[39] A. Grüneis, G. Kresse, Y. Hinuma, and F. Oba, Phys. Rev. Lett. **112**, 096401 (2014).
[40] G. Stefanucci, Y. Pavlyukh, A.-M. Uimonen, and R. van Leeuwen, Phys. Rev. B **90**, 115134 (2014).
[41] M. S. Hybertsen and S. G. Louie, Phys. Rev. B **34**, 5390 (1986).
[42] M. Hindgren and C.-O. Almbladh, Phys. Rev. B **56**, 12832 (1997).
[43] Y. Takada, Phys. Rev. Lett. **87**, 226402 (2001).
[44] A. Marini and A. Rubio, Phys. Rev. B **70**, 081103 (2004).
[45] F. Bruneval, F. Sottile, V. Olevano, R. Del Sole, and L. Reining, Phys. Rev. Lett. **94**, 186402 (2005).
[46] P. Romaniello, S. Guyot, and L. Reining, J. Chem. Phys. **131**, 154111 (2009).
[47] H. Maebashi and Y. Takada, Phys. Rev. B **84**, 245134 (2011).
[48] A. J. Morris, M. Stankovski, K. T. Delaney, P. Rinke, P. García-González, and R. W. Godby, Phys. Rev. B **76**, 155106 (2007).
[49] G. Baym, Phys. Rev. **127**, 1391 (1962).
[50] B. Holm and U. von Barth, Phys. Rev. B **57**, 2108 (1998).
[51] P. García-González and R. W. Godby, Phys. Rev. B **63**, 075112 (2001).
[52] N. E. Dahlen and R. van Leeuwen, J. Chem. Phys. **122**, 164102 (2005).
[53] A. Kutepov, S. Y. Savrasov, and G. Kotliar, Phys. Rev. B **80**, 041103 (2009).
[54] W. Ku and A. G. Eguiluz, Phys. Rev. Lett. **89**, 126401 (2002).
[55] A. Stan, N. E. Dahlen, and R. van Leeuwen, Europhys. Lett. **76**, 298 (2006); J. Chem. Phys. **130**, 114105 (2009).
[56] R. Del Sole and R. Girlanda, Phys. Rev. B **54**, 14376 (1996).
[57] F. Bechstedt, K. Tenelsen, B. Adolph, and R. Del Sole, Phys. Rev. Lett. **78**, 1528 (1997).
[58] M. Rohlfing and S. G. Louie, Phys. Rev. B **62**, 4927 (2000).
[59] M. E. Casida, J. Mol. Struc. THEOCHEM Time-dependent density-functional theory for molecules and molecular solids, **914**, 3 (2009).
[60] G. Onida, L. Reining, and A. Rubio, Rev. Mod. Phys. **74**, 601 (2002).
[61] M. J. T. Oliveira and F. Nogueira, Comput. Phys. Commun. **178**, 524 (2008).
[62] R. Gómez-Abal, X. Li, M. Scheffler, and C. Ambrosch-Draxl, Phys. Rev. Lett. **101**, 106404 (2008); X.-Z. Li, R. Gómez-Abal, H. Jiang, C. Ambrosch-Draxl, and M. Scheffler, New J. Phys. **14**, 023006 (2012).
[63] F. Bruneval, N. Vast, and L. Reining, Phys. Rev. B **74**, 045102 (2006).
[64] S. Lebègue, B. Arnaud, M. Alouani, and P. E. Bloechl, Phys. Rev. B **67**, 155208 (2003).
[65] J. Lischner, S. Sharifzadeh, J. Deslippe, J. B. Neaton, and S. G. Louie, Phys. Rev. B **90**, 115130 (2014).
[66] W. Kang and M. S. Hybertsen, Phys. Rev. B **82**, 195108 (2010).
[67] J. Deslippe, G. Samsonidze, M. Jain, M. L. Cohen, and S. G. Louie, Phys. Rev. B **87**, 165124 (2013).
[68] J. Klimeš, M. Kaltak, and G. Kresse, Phys. Rev. B **90**, 075125 (2014).
[69] W. Kang and M. S. Hybertsen, Phys. Rev. B **82**, 085203 (2010).
[70] S. Sharifzadeh, I. Tamblyn, P. Doak, P. T. Darancet, and J. B. Neaton, Eur. Phys. J. B **85**, 1 (2012).
[71] W. Gao, W. Xia, X. Gao, and P. Zhang, arXiv:1601.06767 [cond-mat, physics:physics] (2016), arXiv: 1601.06767.
[72] P. Baltzer, L. Karlsson, B. Wannberg, G. Öhrwall, D. M. P. Holland, M. A. MacDonald, M. A. Hayes, and W. von Niessen, Chem. Phys. **224**, 95 (1997).
[73] P. M. Mayer, V. Blanchet, and C. Joblin, J. Chem. Phys. **134**, 244312 (2011).
[74] N. Kishimoto, H. Yamakado, and K. Ohno, J. Phys. Chem. **100**, 8204 (1996).
[75] T. Pasinszki, M. Krebsz, and G. Vass, J. Mol. Struct. **966**, 85 (2010).
[76] P. Rademacher, K. Kowski, A. Müller, and G. Bohlmann, J. Mol. Struct. **296**, 115 (1993).
[77] A. J. Berlinsky, J. F. Carolan, and L. Weiler, Can. J. Chem. **52**, 3373 (1974).
[78] P. D. Burrow, J. A. Michejda, and K. D. Jordan, J. Chem. Phys. **86**, 9 (1987).
[79] B. Hajgató, M. S. Deleuze, D. J. Tozer, and F. De Proft, J. Chem. Phys. **129**, 084308 (2008).
[80] H. H. Falden, K. R. Falster-Hansen, K. L. Bak, S. Rettrup, and S. P. A. Sauer, J. Phys. Chem. A **113**, 11995 (2009).
[81] H. Fliegl and D. Sundholm, Phys. Chem. Chem. Phys. **16**, 9859 (2014).
[82] M. Stenrup, Chem. Phys. **397**, 18 (2012).
[83] M. H. Palmer, Chem. Phys. **348**, 130 (2008).
[84] D. J. Tozer and N. C. Handy, J. Chem. Phys. **109**, 10180 (1998).
[85] M. E. Casida, C. Jamorski, K. C. Casida, and D. R. Salahub, J. Chem. Phys. **108**, 4439 (1998).

[86] S. S. Leang, F. Zahariev, and M. S. Gordon, J. Chem. Phys. **136**, 104101 (2012).
[87] A. D. Laurent and D. Jacquemin, Int. J. Quantum Chem. **113**, 2019 (2013).
[88] S. Refaely-Abramson, R. Baer, and L. Kronik, Phys. Rev. B **84**, 075144 (2011).